Yang, L.; Huang, Y.; Peng, Q.; Feyerabend, F.; Kainer, K.U.;
Willumeit, R.; Hort, N.:

Mechanical and Corrosion Properties of Binary Mg-Dy Alloys for Medical Application

In: Materials Science and Engineering B (2011) Elsevier

DOI: 10.1016/j.mseb.2011.02.025

Mechanical and Corrosion Properties of Binary Mg-Dy Alloys for Medical Application

Lei Yang*, Yuanding Huang, Qiuming Peng, Frank Feyerabend, Karl Ulrich Kainer, Regine Willumeit, Norbert Hort

GKSS Research Centre, Institute of Materials Research, Max-Planck-Str. 1, D-21502 Geesthacht, Germany

Abstract

Microstructure, mechanical and corrosion properties of binary magnesium-dysprosium (Mg-xDy; with x=5, 10, 15 and 20 wt.%) alloys were investigated for medical applications. In the as-cast condition, Mg-10Dy alloy exhibits the best combination of mechanical and corrosion properties. The mechanical properties of Mg-Dy alloys decrease after solution treatment due to the dissolution of precipitates and increase of grain size. However, corrosion properties are significantly improved as a result of the reduction of both filiform and pitting corrosion. Aging at 250^{o}C has no significant effect on the mechanical and corrosion properties. The corrosion of Mg-Dy alloys is influenced by the distribution of Dy in the alloys. The solution of Dy in Mg matrix reduces the filiform corrosion, while its existence in the form of $Mg_{24}Dy_5$ precipitates accelerates the pitting corrosion.

Keywords: Magnesium, Dysprosium, biomaterials, mechanical property, corrosion

* Corresponding author. Address: GKSS Research Centre, Magnesium Innovation Centre, Institute of Materials Research, Max-Planck-Str. 1, D-21502 Geesthacht, Germany. Tel.: +49 4152 87 1923; fax: +49 4152 87 1909.

E-mail address: lei.yang@gkss.de

1 Introduction

Magnesium is increasingly attracting attention as an interesting candidate for degradable implants in the human body. The most attractive point is that there will be no need for a second surgery to remove the implants, which is necessary for implants based on stainless steel or titanium. In addition, the young's modulus and mechanical properties of Mg and its alloys are very close to that of natural bone, and the level of Mg in body can be maintained by the kidneys and intestine [1, 2].

However, to be applied as degradable implants, Mg alloys must fulfil certain requirements: (i) appropriate mechanical characteristics, such as sufficient ductility for ease of fabrication and proper strength to offer adequate mechanical support to the injured tissue; (ii) a moderate and homogeneous degradation rate to maintain the mechanical integrity of the implant during the healing process; and (iii) good biocompatibility, which is the most important.

Recently, several Mg alloys have been studied as biomaterials, including AZ31 [3], AZ91 [3-6], WE43 [3], LAE442 [3, 4, 7], Mg-Ca [8-10], Mg-Zn [11], Mg-Mn-Zn [12, 13], Mg-Si-Ca [14], Mg-Si-Zn [14], Mg-Mn-Zn-Ca [15]. In some studies, rare earth-containing Mg alloys (Mg-RE) are believed to be suitable for biomedical application, and some of them exhibit both good mechanical and corrosion properties [3, 7, 16, 17]. Unfortunately, although Mg-RE alloys exhibit excellent mechanical and corrosion properties, the previously developed Mg-RE alloys were mainly intended for structural uses and some elements in them are unsuitable for biomedical applications. For example, La and Ce showed high cytotoxicity in *in vitro* studies and they were suggested to be used cautiously [18]. Moreover, the Mg-RE alloys tested for medical application are prepared via master alloys. As a result, besides the nominal

composition, several other elements and impurities are contained in the alloy [18]. Therefore, the development of new Mg-RE alloys with good biocompatibility, mechanical and corrosion properties is necessary.

The investigation of Mg-Gd alloys showed that their properties are very close to the values of cortical bone. Furthermore, their TYS, UTS, CYS and UCS can be adjusted over a wide range, which makes them promising candidates for the future design of degradable metallic implants [19]. Dy shows good cytocompatibility according to the in vitro study of cytotoxicity and inflammatory response [18], and the half-lethal dose (LD50) value of Dysprosium chloride is 585 mg/kg [20]. Furthermore, the use of dysprosium compounds as negative contrast agents for high field magnetic resonance imaging is attracting growing attention[21]. In addition, due to the high solubility of Dy in Mg (25.3wt. %), it is possible to adjust both mechanical and corrosion properties through the control of Dy content or heat treatment. Hence, Dy is considered as a potential alloying element for the design of new Mg-RE based implants.

In this work, Mg-xDy(x=5, 10, 15 and 20 in wt.%) alloys were fabricated and their mechanical and corrosion properties were studied. These basic data will provide information needed to optimize the new implant materials in future.

2 Experimental procedures

2.1 Material preparation

High-purity Mg was molten in a mild steel crucible under a protective atmosphere (Ar + 2% SF6). Pure Dy was added at a melt temperature of 720 ^{o}C in amounts of 5, 10, 15 and 20wt.%. The melt was stirred for 30 min at 200 rpm. After that, the melt was cast with directly chilled permanent mould casting method. Firstly, the melt was

poured into a mould preheated at 500 ^{o}C. Then the filled mould was held at 670 ^{o}C for 30 min under protective gas. After that the whole steel crucible with the melt was immersed into the continuous cooling water at a rate of 10 mm/s. When the bottom of steel crucible touched the water, it was stopped for 1 second. As soon as the liquid level of inside melt was in alignment with the height of outside water, the solidification process was finished. The size of ingot is 6 cm×12 cm×20 cm.

The chemical compositions of the alloys were analyzed using inductively coupled plasma–optical emission spectroscopy ICP-OES (Spectroflame, Spectro, Kleve, Germany), as listed in Table 1. Solution treatment was done under 520^{o}C for 24h, and then the ingots were quenched into water. Aging at 250 ^{o}C for 16h was chosen as the T6 treatment.

2.2 Microstructure

Specimens were prepared using electrochemical polishing method. Microstructure was investigated using a high-resolution scanner and a Zeiss Ultra 55 (Carl Zeiss GmbH, Oberkochen, Germany) scanning electron microscopy (SEM) equipped with energy dispersive X-ray analysis (EDX). Grain sizes were determined using the line intercept method [22].

2.3 Mechanical properties

Tension and compression tests were performed at room temperature using a Zwick 050 testing machine (Zwick GmbH & Co., KG, Ulm, Germany) according to DIN EN 10002 [23] and DIN 50106 [24]. Specimens with a gauge length of 30 mm, a diameter of 6 mm and threaded heads were used in the tension tests. The compression specimens were cylinders with a length of 16.5 mm and a diameter of 11 mm. Both tension and compression tests were done under a strain rate of 1×10^{-3}s.

At least three specimens were tested under each condition.

2.4 Corrosion

The hydrogen (H_2) evolution measurement of the alloys was investigated by immersion tests in standard eudiometer set-ups with a total volume of 400 ml and a resolution of 5 ml. The tests were performed in physiological saline (0.9 wt. % NaCl solution) at room temperature. The specimen were prepared by grinding each side with 2400 grid emery paper and degreasing the surfaces with ethanol prior to corrosion testing. The hydrogen evolution as an indicator of the corrosion rate was monitored. The average corrosion rate of each specimen at the end of the tests was calculated in millimetre per year by converting the total amount of collected hydrogen into material loss (1 ml H_2 gas = 0.001083 g dissolved Mg) and using the following equation (weight change Δg in g, surface area A in cm^2, time t in h, density of the alloy ρ in g cm^{-3}):

$$CR = \frac{8.76 \times 10^4 \times \Delta \mathrm{g}}{\mathrm{A} \cdot t \cdot \rho}$$

At least two samples were used in this experiment. In order to understand the corrosion mechanism, the corrosion morphology was observed.

3 Results

3.1 Microstructure

Fig. 1 shows the optical microstructure of Mg-Dy alloys in as-cast (F) condition. Very inhomogeneous microstructure is formed due to the fast solidification during the casting process. The grain size decreases significantly with the addition of Dy from 5 wt.% to 10 wt.%, but further addition of Dy barely refines the grain as shown in Table 2. Fig. 2 illustrates the distribution of Dy and morphology of second phase in Mg-Dy

alloys. The bright area is the segregation of Dy distributing mainly at the interdendritic region and the grain boundaries. With the increase of Dy content, the segregation of Dy and amount of second phases increase. When Dy content reaches to 20 wt.%, the amount of second phases increases apparently. The distribution of Dy in different regions of Mg-Dy alloys was analyzed using EDX, as listed in Table 3. The Dy content in matrix (as indicated by arrow A) is about half its designed content in alloys. For example, 2.17 wt.% and 10.3 wt.% Dy were identified in the matrix of Mg-5Dy and Mg-20Dy alloys, respectively. The Dy content at the interdendritic region (as indicated by arrow B) is much higher than that in the matrix and increases gradually with the increment of Dy. For example, it increases from 19.26 wt.% to 29.2 wt.% when Dy increases from 5 to 20 wt.% in the alloys. Fig. 2(e) shows the morphology of second phases in Mg-20Dy alloy. According to EDX analysis, the composition of the second phase is about 85% Mg, 14% Dy and 1% O in atomic percent. Thus, we can deduce that it is $Mg_{24}Dy_5$ phase based on Mg/Dy atomic ratio and Mg-Dy binary phase diagram [25].

After solution treatment, the grain size increases generally. However, the value of grain size in Table 2 can only be regarded as a reference because of the microstructural inhomogeneity. Fig. 3 shows the microstructure of Mg-Dy alloys after T4 treatment. The dendrites disappear completely and only extremely few precipitates remain in the alloys. The Dy content in the matrix was analyzed using EDX (arrow D). As listed in Table 3, the Dy content in the matrix of Mg-5Dy, Mg-10Dy, Mg-15Dy and Mg-20Dy alloys are 4.38, 8.23, 12.38 and 18.01, respectively. This indicates that most of Dy element dissolves into the Mg matrix, which is consistent with the microstructure.

3.2 Mechanical properties

Fig. 4 shows the mechanical properties of Mg-Dy alloys at room temperature. Tensile yield strength (TYS) of Mg-Dy alloys in different conditions is illustrated in Fig. 4(a). In the F condition, TYS is enhanced significantly with the increase of Dy content, and reaches to 112 MPa for Mg-20Dy alloy. After T4 treatment, the TYS of all alloys decreases, especially for Mg-10Dy and Mg-15Dy alloys reducing from 82 MPa and 105 MPa to 63 MPa and 68 MPa, respectively. After T6 treatment, slight improvements of TYS are obtained for Mg-10Dy, Mg-15Dy and Mg-20Dy alloys, but apparent decrease (from 40 to 30MPa) was noticed for Mg-5Dy alloy. Similar results to TYS were found in compression yield strength (CYS) as shown in Fig. 4(b).

Ultimate tensile strength (UTS) of Mg-Dy alloys in different conditions is shown in Fig. 4(c). In the F condition, Mg-5Dy shows the lowest UTS, about 77MPa. With the addition of Dy content up to 10 wt.%, the UTS is improved significantly, reaching 130MPa. However, UTS maintains at the same level with the further increase of Dy content. After T4 treatment, little change is observed for UTS of Mg-5Dy, Mg-15Dy and Mg-20Dy alloy, but the UTS of Mg-10Dy alloy declines remarkably. Even after T6 treatment, no improvement was obtained in UTS for all alloys. Fig. 4(d) illustrates the ultimate compression strength (UCS) of Mg-Dy alloys. Different from TYS, the UCS increases linearly with the increase of Dy content in F condition. The highest UTCS (about 290 MPa) is observed in Mg-20Dy alloy. After T4 treatment, the UCS of Mg-5Dy alloy remains unchanged. However, the UCS of other Mg-Dy alloys reduces significantly, especially for Mg-20Dy alloy decreasing from 290 MPa to 190 MPa. After T6 treatment, only slight improvements are obtained. Thus, the UCS seems to be more sensitive to heat treatment than UTS.

Fig. 4(e) shows the elongation to fracture of Mg-Dy alloys. The broad error bars are obtained due to the inhomogeneity of microstructure. In F condition, Elongation

increases a little with the addition of Dy increasing from 5 wt.% to 10 wt.%, while it declines dramatically when Dy content increases to 15 wt.% and 20 wt.%. Heat treatment shows no significant effects on the elongation which is still at the same level with that in F condition.

3.3 Corrosion

Fig. 5 shows the corrosion rate of Mg-Dy alloys in 0.9 wt.% NaCl solution at room temperature. In the F condition, Mg-10Dy alloy exhibits the lowest corrosion rate in physiological saline (about 3mm/year), which is less than half of the corrosion rate of Mg-5Dy alloy. Further increase in Dy content slightly increases the corrosion rate of F Mg-Dy alloys. After T4 treatment, the corrosion rate of all alloys is significantly reduced, especially for Mg-5Dy alloy decreasing from 7.9mm/year to 0.5mm/year. The corrosion rates of Mg-10Dy and Mg-15Dy alloys are about 0.8 mm/year, which is slightly higher than that of Mg-5Dy alloy. However, the corrosion rate increases suddenly in Mg-20Dy alloy, reaching 2.2 mm/year. After T6 treatment, corrosion rate is further reduced for Mg-Dy alloys with less than 15 wt.% Dy; a small increase was found in the Mg-20Dy alloy.

The typical corrosion morphologies of F alloys are shown in Fig. 6. Apparent filiform corrosion occurs on the surface of the Mg-5Dy alloy after 72h immersion testing (Fig. 6(a)), which diminished significantly with an increase in Dy content. When Dy content is more than 15 wt.%, no filiform corrosion is observed (Fig. 6 (c, d)). In the mean time, with the increase of Dy, pitting corrosion increases. Both the filiform and pitting corrosion lead to high corrosion rate. As a result, the lowest corrosion rate is obtained in Mg-10Dy alloy due to the balance between the pitting and filiform corrosion. After T4 treatment, the variation of pitting and filiform corrosion is similar to that in F condition. The filiform corrosion decreases but the pitting

corrosion increases with the increase of Dy content as shown in Fig. 7. However, both of pitting and filiform corrosion are reduced apparently compared with it in F condition, which agreed with the results of corrosion rate.

4 Discussion

4.1 Microstructure and mechanical properties

Based on the Mg–Dy binary phase diagram [25] the maximum solid solubility of Dy is 25.3 wt.% in Mg matrix at 561^{o}C. Due to the special casting technique in this work, the solidification process was completely under a non-equilibrium condition. As a result, besides the Dy in Mg matrix, large amount of Dy exists at the segregation areas and only a small amount of Dy precipitates as second phase. According to Mg-Dy binary phase diagram and EDX results, the precipitates were confirmed to be the $Mg_{24}Dy_5$ phase.

The improvement of TYS in Mg-Dy alloys can be mostly attributed to solid-solution strengthening and precipitate strengthening. With the increase of Dy content, the fraction of eutectic phase and Dy content in Mg matrix increases. As a result, both precipitate strengthening and solid-solution strengthening effects are improved. Thus, the apparent improvement in YS was obtained with the increase of Dy in Mg-Dy alloys. The slight improvement in elongation is found when Dy increases from 5 wt.% to 10 wt.%, which is mainly from the contribution of grain refinement. However, the further addition of Dy only results in the increase of intermetallic phases and Dy solubility in Mg matrix, but barely grain refinement effect. Hence, elongation of Mg-15Dy and Mg-20Dy alloy decreases sharply. After T4 treatment, the loss of strength is mainly attributed to the dissolution of precipitates. Meanwhile, the increase in grain size is another reason. T6 treatment shows no significant effects both on mechanical

and corrosion properties. The reason could be only small amount of nano-scaled phase precipitated out because of the high solubility of Dy in Mg, which could reach 12 wt.% even if at 250^{o}C [25].

4.2 Corrosion

Based on the corrosion morphologies as shown in Fig. 6 and Fig. 7, it can be concluded that the different contents and existence forms of Dy in Mg-Dy alloys could directly result in different corrosion mechanisms, namely filiform and/or pitting corrosion.

Filiform corrosion is caused by active galvanic cells across the metal surface. Its head is anodic, whereas the tail is cathodic. It is typically associated with metal surfaces having an applied protective coating [26]. For Mg alloys, filiform corrosion has already been observed in NaCl solutions in several studies [27-30]. However, the detailed mechanism is still not well understood. For Mg-Dy alloys, it is found that the filiform corrosion is affected by Dy content in the Mg matrix. The increase of Dy content in the alloys diminishes filiform corrosion effectively due to the increase of Dy in Mg Matrix as shown in Fig. 6. After T4 treatment, the content of Dy in Mg matrix increases significantly. As a result the filiform corrosion is reduced significantly as shown in Fig. 7. The reason for the reduction of filiform corrosion with the increase of Dy could be (i) the corrosion resistance of matrix is improved due to the dissolution of Dy; (ii) the protective corrosion film with more corrosion-resistant ability could be formed in high Dy-containing alloy. The phenomenon that the dissolution of alloying elements could influence the occurrence of filiform corrosion was also reported in Mg-Zn-Y alloy [29]. It was reported that in the as-solidified alloys, an increase in the cooling rate brought a delay in the occurrence of filiform corrosion, and it is attributed to grain refinement and formation of a supersaturated single Mg phase solid solution

in the alloys. In order to understand the mechanism of solubility of alloying elements on filiform corrosion, further investigations have to be carried out.

Normally, the second phase or compound in Mg alloys is inert and stable compared to Mg matrix in corrosion process. In AZ91 alloy a large amount of $Mg_{17}Al_{12}$ phase with network structure can be a corrosion barrier to retard the corrosion; however, a small amount of $Mg_{17}Al_{12}$ phases acts as a cathode and form galvanic couples with the Mg matrix, accelerating the corrosion rate [31, 32]. Thus it can be deduced that the pitting corrosion in Mg-Dy alloys primarily starts from the $Mg_{24}Dy_5$ phase which forms galvanic couples with the Mg matrix. As a result, more pitting corrosion occurs with the increase of Dy content in the F condition due to the formation of more eutectic phases. After T4 treatment, few precipitates remain in Mg-Dy alloys with less than 15 wt.% Dy. Therefore, the corrosion rates are reduced largely. However, for Mg-20Dy alloy, much pitting corrosion happens because a few precipitates still remain there.

5 Conclusion

1. In the as-cast condition, tensile and compression yield strengths are enhanced significantly with the increase of Dy content due to the main solid solution of Dy and part of precipitation strengthening. Mg-10 Dy alloy exhibits the best combination of tensile, compression and corrosion properties.
2. After solution treatment the strengths are more or less deteriorated due to the dissolution of precipitates and the increase of grain size, but the corrosion resistance is improved significantly. The present aging treatment shows no apparent effects on both the mechanical and corrosion properties.
3. The corrosion of Mg-Dy alloys are related to two corrosion mechanisms: filiform and pitting corrosions, both of which are influenced by the distribution of Dy. The

solution of Dy in Mg matrix reduces the filiform corrosion effectively, but its existence in the form of $Mg_{24}Dy_5$ precipitates accelerates the pitting corrosion.

Acknowledgement

The authors express their gratitude to Dr. Jun Liang for thoughtful discussions. Technical support from Volker Kree, Willi Punessen is acknowledged. Financial support from CSC-Helmholtz scholarship for Yang′ s PhD study in GKSS Research Centre is appreciated.

References

[1] M. P. Staiger, A. M. Pietak, J. Huadmai, G. Dias, Biomaterials 27 (2006) 1728-1734.

[2] F. Witte, N. Hort, C. Vogt, S. Cohen, K. U. Kainer, R. Willumeit, F. Feyerabend, Curr. Opin. Solid State Mater. Sci. 12 (2008) 63-72.

[3] F. Witte, V. Kaese, H. Haferkamp, E. Switzer, A. Meyer-Lindenberg, C. J. Wirth, H. Windhagen, Biomaterials 26 (2005) 3557-3563.

[4] F. Witte, J. Fischer, J. Nellesen, H. A. Crostack, V. Kaese, A. Pisch, F. Beckmann, H. Windhagen, Biomaterials 27 (2006) 1013-1018.

[5] F. Witte, H. Ulrich, M. Rudert, E. Willbold, J. Biomed. Mater. Res. 81A (2007) 748-756.

[6] F. Witte, F. Feyerabend, P. Maier, J. Fischer, M. Störmer, C. Blawert, W. Dietzel, N. Hort, Biomaterials 28 (2007) 2163-2174.

[7] F. Witte, J. Fischer, J. Nellesen, C. Vogt, J. Vogt, T. Donath, F. Beckmann, Acta Biomater. 6 (2010) 1792-1799.

[8] Z. Li, X. Gu, S. Lou, Y. Zheng, Biomaterials 29 (2008) 1329-1344.

[9] W.-C. Kim, J.-G. Kim, J.-Y. Lee, H.-K. Seok, Materials Letters 62 (2008) 4146-4148.

[10] Y. Wan, G. Xiong, H. Luo, F. He, Y. Huang, X. Zhou, Mater. Des. 29 (2008) 2034-2037.

[11] S. Zhang, X. Zhang, C. Zhao, J. Li, Y. Song, C. Xie, H. Tao, Y. Zhang, Y. He, Y. Jiang, Y. Bian, Acta Biomater. 6 (2010) 626-640.

[12] L. Xu, F. Pan, G. Yu, L. Yang, E. Zhang, K. Yang, Biomaterials 30 (2009) 1512-1523.

[13] E. Zhang, D. Yin, L. Xu, L. Yang, K. Yang, Mater. Sci. Eng. C 29 (2009) 987-993.

[14] E. Zhang, L. Yang, J. Xu, H. Chen, Acta Biomater. 6 (2010) 1756-1762.

[15] E. Zhang, L. Yang, Mater. Sci. Eng. A 497 (2008) 111-118.

[16] A. C. Hanzi, P. Gunde, M. Schinhammer, P. J. Uggowitzer, Acta Biomater. 5 (2009) 162-171.

[17] P. Gunde, A. Furrer, A. C. Häzi, P. Schmutz, P. J. Uggowitzer, J. Biomed. Mater. Res. 92A (2010) 409-418.

[18] F. Feyerabend, J. Fischer, J. Holtz, F. Witte, R. Willumeit, H. Drückere, C. Vogt, N. Hort, Acta Biomater. 6 (2010) 1834-1842.

[19] N. Hort, Y. Huang, D. Fechner, M. Stömer, C. Blawert, F. Witte, C. Vogt, H. Drüker, R. Willumeit, K. U. Kainer, F. Feyerabend, Acta Biomater. 6 (2010) 1714-1725.

[20] T. J. Haley, L. Koste, N. Komesu, M. Efros, H. C. Upham, Toxicol. Appl. Pharmacol. 8 (1966) 37-43.

[21] M. Bottrill, L. K. Nicholas, N. J. Long, Chem. Soc. Rev. 35 (2006) 557-571.

[22] ASTM E112. Standard test methods for determining average grain size. doi: 10.1520/E0112-96R04E02.

[23] DIN EN ISO 10002. Tension testing of metallic materials. Berlin: Beuth Verlag; 2001.

[24] DIN 50106. Compression testing of metallic materials. Berlin, Germany: Beuth Verlag;1978.

[25] A. A. Nayeb-Hashemi, J. B. Clark, Phase Diagram of Binary Magnesium Alloys, ASM International, Metal Park, OH, USA, 1988.

[26] R. C. Zeng, J. Zhang, W. J. Huang, W. Dietzel, K. U. Kainer, C. Blawert, W. Ke, Trans. Nonferrous Met. Soc. China 16 (2006) 763-771.

[27] Y. Song, D. Shan, R. Chen, E.-H. Han, Corros. Sci. 52 (2010) 1830-1837.

[28] Y. Song, D. Shan, R. Chen, E.-H. Han, Corros. Sci. 51 (2009) 1087-1094.

[29] S. Izumi, M. Yamasaki, Y. Kawamura, Corros. Sci. 51 (2009) 395-402.

[30] N. Hara, Y. Kobayashi, D. Kagaya, N. Akao, Corros. Sci. 49 (2007) 166-175.

[31] G. Song, A. Atrens, Adv. Eng. Mater. 5 (2003) 837-858.

[32] G. Song, A. Atrens, M. Dargusch, Corros. Sci. 41 (1998) 249-273.

Table captions:

Table 1 Chemical composition of experiment alloys determined by ICP-OES (wt.%).

Table 2 Grain size of Mg-Dy alloys at the edge of cast ingots (mm).

Table 3 Distribution of Dy in different areas of Mg-Dy alloys (wt.%).

Figure captions:

Fig. 1. Optical microstructure of Mg-Dy alloys (a) Mg-5Dy; (b) Mg-10Dy; (c)Mg-15Dy; (d) Mg-20Dy.

Fig. 2. Microstructure of Mg-Dy alloys (a) Mg-5Dy; (b) Mg-10Dy; (c) Mg-15Dy; (d) Mg-20Dy; (e) High magnification of second phase in Mg-20Dy alloys.

Fig. 3. Microstructure of Mg-Dy alloys after T4 treatment ($520^{o}C$+24h) (a) Mg-5Dy; (b) Mg-10Dy; (c) Mg-15Dy; (d) Mg-20Dy.

Fig. 4. Mechanical properties of Mg-Dy alloys (a) Tensile yield strength; (b) Compression yield strength; (c) Ultimate tensile strength; (d) Ultimate compression yield strength; (e) Elongation; (f) Compression deformation.

Fig. 5. Corrosion rates of Mg-Dy alloys after 72h immersion in 0.9wt.% NaCl solution at room temperature. The average corrosion rates were calculated from the hydrogen evolution results.

Fig. 6. Typical corrosion morphology of as-cast Mg-Dy alloys after 72h immersion in 0.9wt. % NaCl solution at room temperature and removing the corrosion products (a) Mg-5Dy alloy; (b) Mg-10Dy alloy; (c) Mg-15Dy alloy; (d) Mg-20Dy alloy.

Fig. 7. Typical corrosion morphology of Mg-Dy alloys (T4) after 72h immersion in 0.9wt.% NaCl solution at room temperature and removing corrosion products, (a) Mg-5Dy alloy; (b) Mg-10Dy alloy; (c) Mg-15Dy alloy; (d) Mg-20Dy alloy.

Figure 1

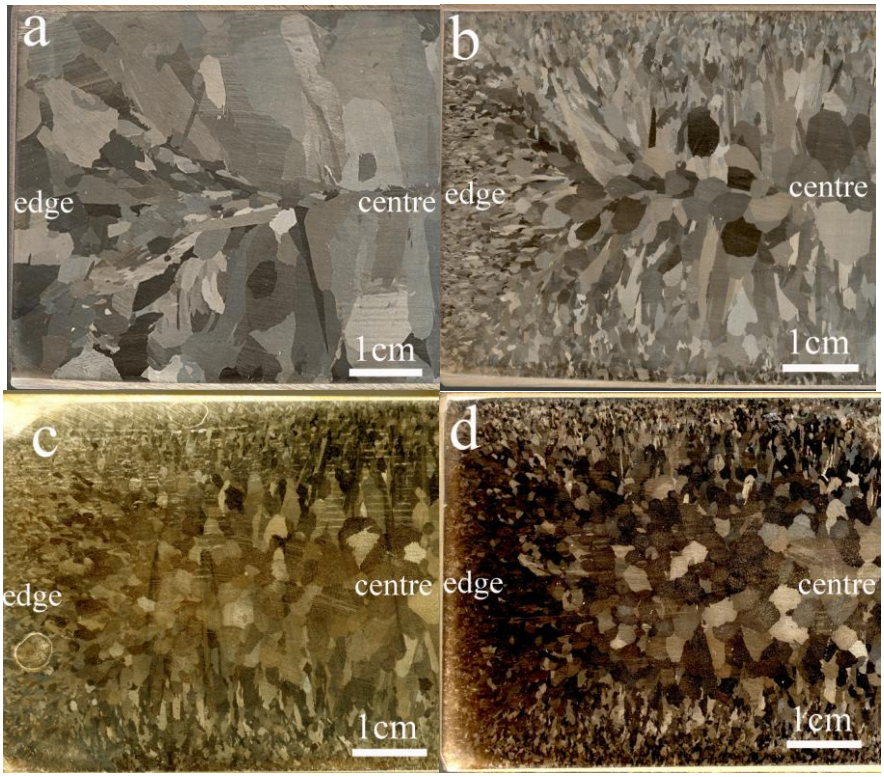

Fig.1. Optical microstructure of Mg-Dy alloys (a) Mg-5Dy; (b) Mg-10Dy; (c)Mg-15Dy; (d) Mg-20Dy.

Figure 2

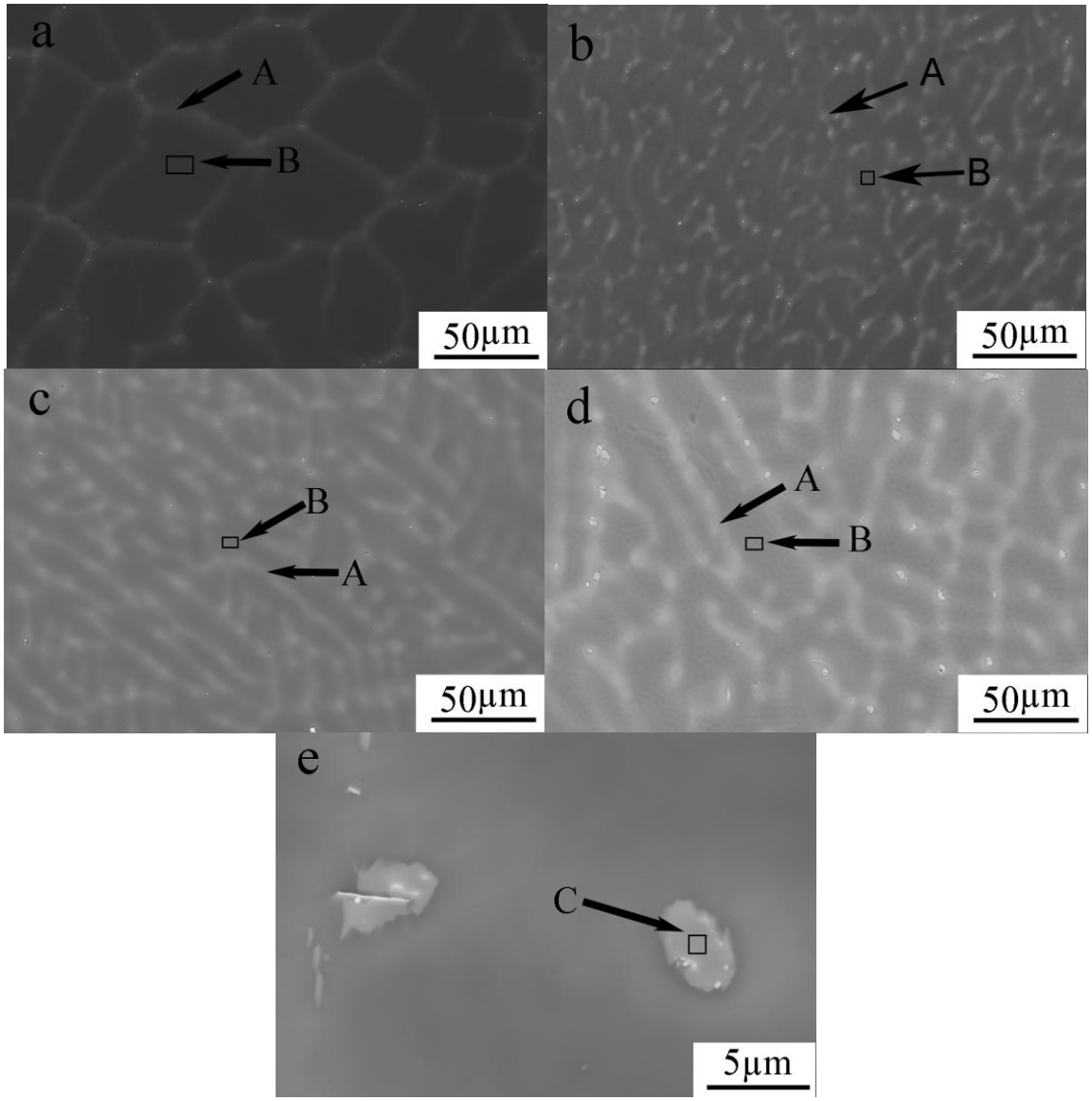

Fig. 2. Microstructure of Mg-Dy alloys (a) Mg-5Dy; (b) Mg-10Dy; (c) Mg-15Dy; (d) Mg-20Dy; (e) High magnification of second phase in Mg-20Dy alloys.

Figure 3

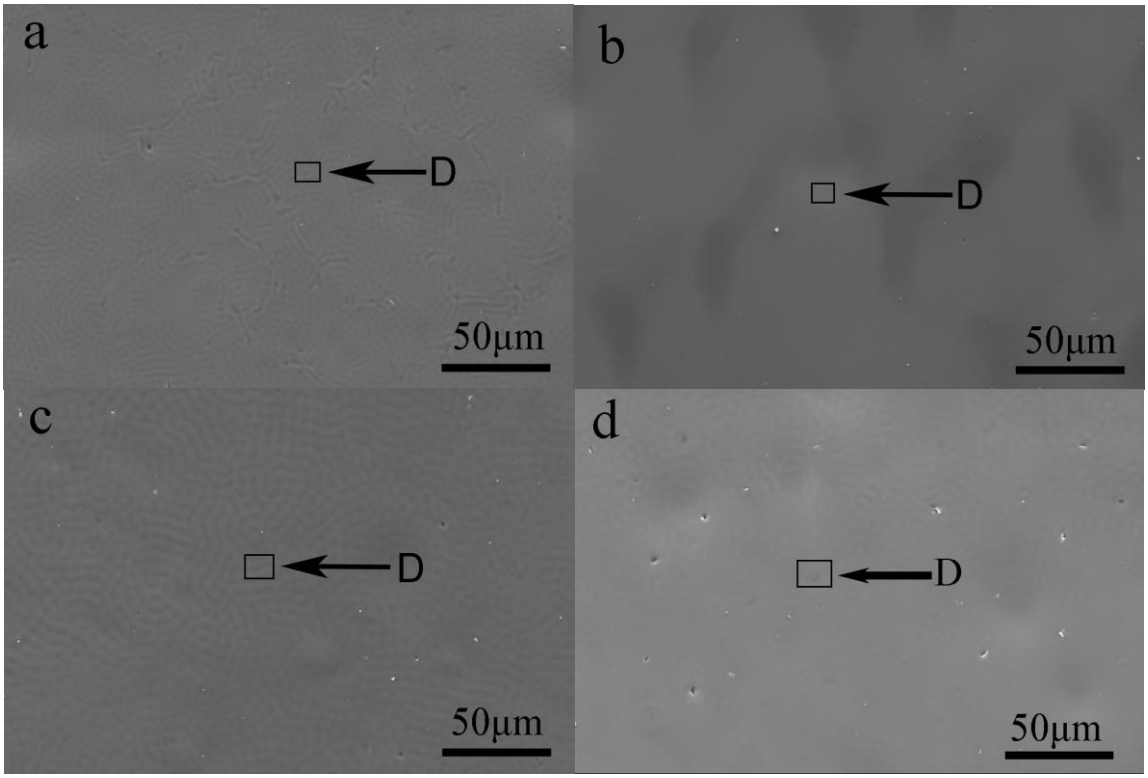

Fig. 3. Microstructure of Mg-Dy alloys after T4 treatment (520^{o}C+24h) (a) Mg-5Dy; (b) Mg-10Dy; (c) Mg-15Dy; (d) Mg-20Dy.

Figure 4

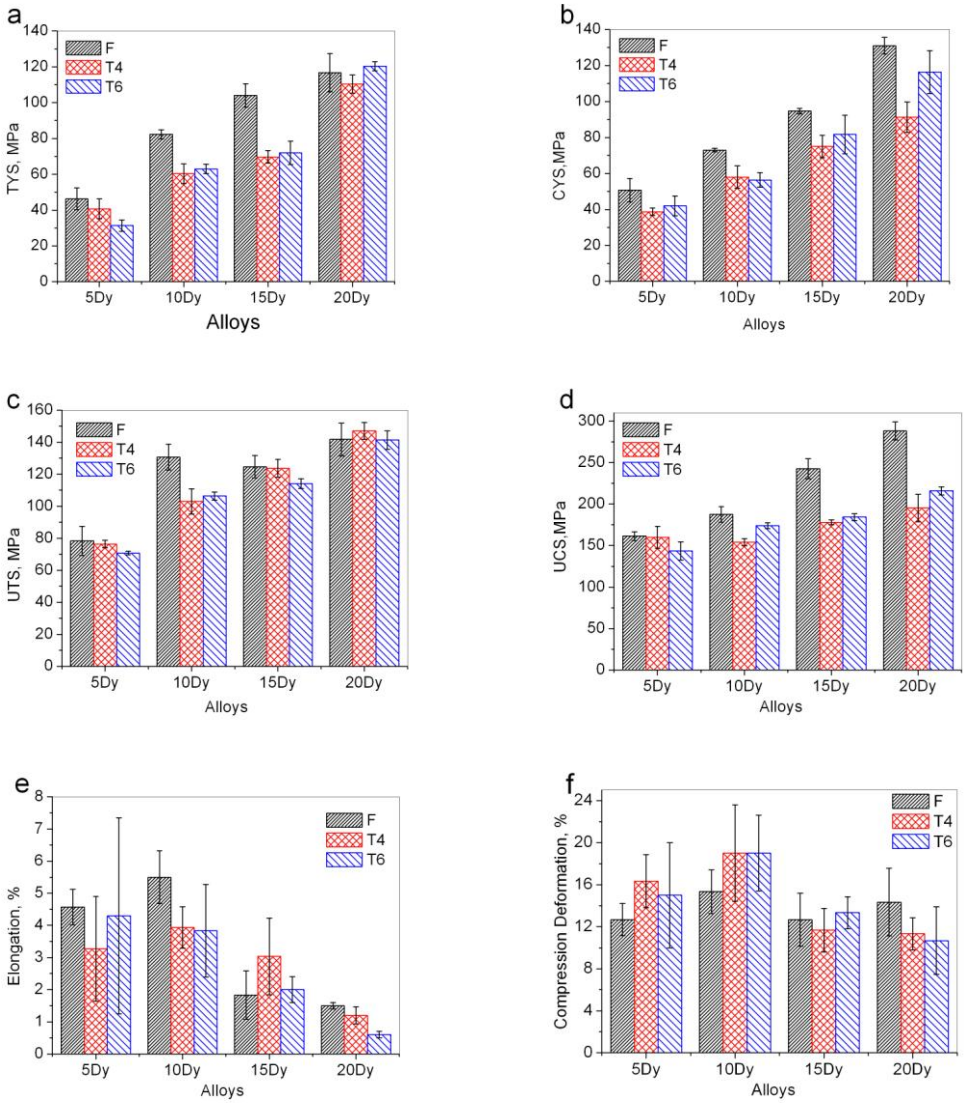

Fig. 4. Mechanical properties of Mg-Dy alloys (a) Tensile yield strength; (b) Compression yield strength; (c) Ultimate tensile strength; (d) Ultimate compression yield strength; (e) Elongation; (f) Compression deformation.

Figure 5

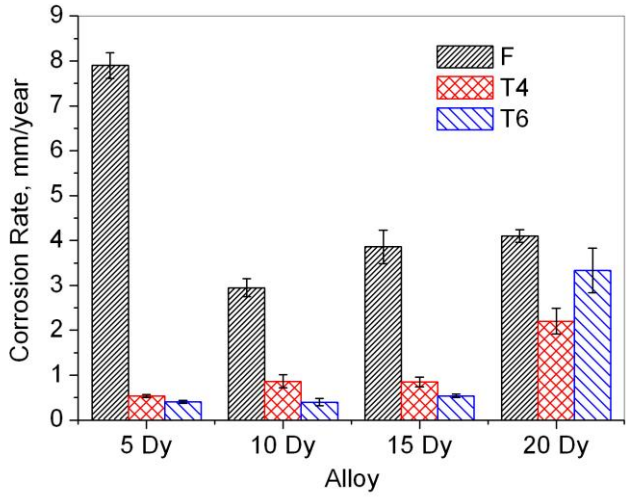

Fig. 5. Corrosion rates of Mg-Dy alloys after 72h immersion in 0.9wt.% NaCl solution at room temperature. The average corrosion rates were calculated from the hydrogen evolution results.

Figure 6

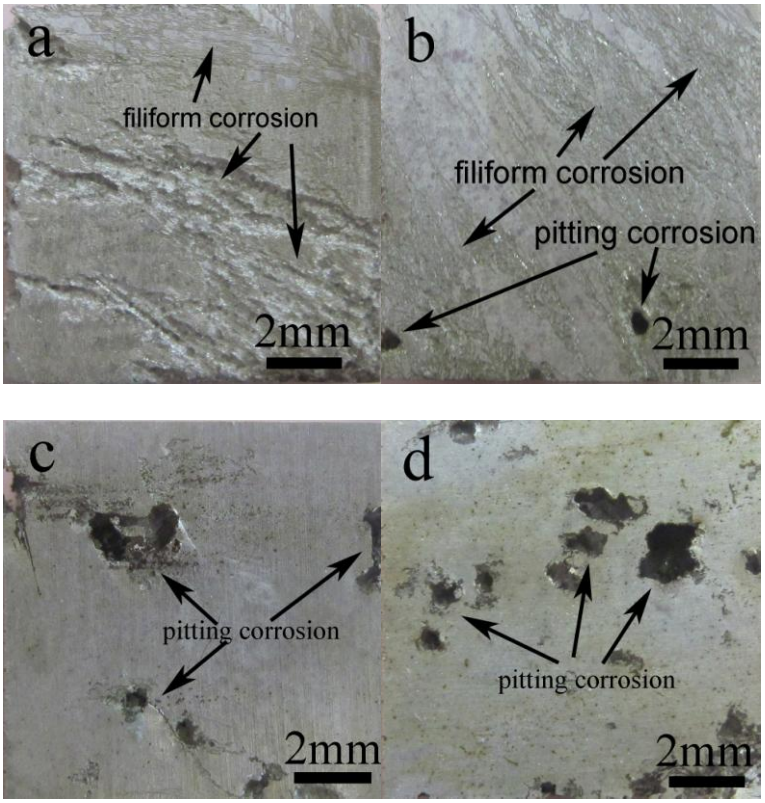

Fig. 6. Typical corrosion morphology of as-cast Mg-Dy alloys after 72h immersion in 0.9wt. % NaCl solution at room temperature and removing the corrosion products (a) Mg-5Dy alloy; (b) Mg-10Dy alloy; (c) Mg-15Dy alloy; (d) Mg-20Dy alloy.

Figure 7

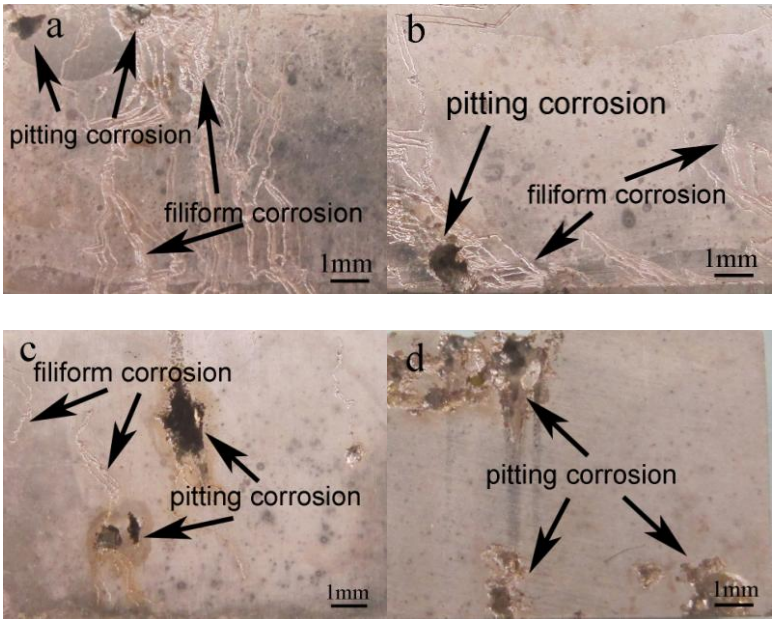

Fig. 7. Typical corrosion morphology of Mg-Dy alloys (T4) after 72h immersion in 0.9wt.% NaCl solution at room temperature and removing corrosion products, (a) Mg-5Dy alloy; (b) Mg-10Dy alloy; (c) Mg-15Dy alloy; (d) Mg-20Dy alloy.

Table 1

Table 1 Chemical composition of experiment alloys determined by ICP-OES (wt.%).

Alloy	Dy	Fe	Ni	Cu	Mg
Mg-5Dy	4.5	0.025	<0.01	<0.01	Balance
Mg-10Dy	8.7	0.033	<0.01	<0.01	Balance
Mg-15Dy	13.1	0.023	<0.01	<0.01	Balance
Mg-20Dy	18.9	0.043	<0.01	<0.01	Balance

Table 2

Table 2 Grain size of Mg-Dy alloys at the edge of cast ingots (mm).

Alloy	Mg-5Dy	Mg-10Dy	Mg-15Dy	Mg-20Dy
Edge (F)	3.34±2.87	0.61±0.46	0.56±0.26	0.64±0.23
Edge (T4)	3.82±4.14	1.23±0.68	0.79±0.44	0.52±0.43
T6	---	---	---	---

Table 3

Table 3 Distribution of Dy in different areas of Mg-Dy alloys (wt.%).

alloys	Mg-5Dy	Mg-10Dy	Mg-15Dy	Mg-20Dy
Matrix (F)	2.17	4.88	7.6	10.3
Interdendritic region (F)	19.26	21.43	25.85	29.2
Phase (F)	---	---	---	52.4
Matrix (T4)	4.38±0.049	8.23±0.035	12.38±0.25	18.01±0.18